UC Riverside

UC Riverside Previously Published Works

Title

Lipid and protein corona of food-grade TiO2 nanoparticles in simulated gastrointestinal digestion

Permalink

https://escholarship.org/uc/item/1ds5c3nf

Authors

Coreas, Roxana
Cao, Xiaoqiong
Deloid, Glen M
et al.

Publication Date

DOI

Peer reviewed

Lipid and protein corona of food-grade TiO₂ nanoparticles in simulated gastrointestinal digestion

Roxana Coreas[1], Xiaoqiong Cao[2], Glen M. Deloid[2], Philip Demokritou[2,*], Wenwan Zhong[1,3,*]

[1]Environmental Toxicology Graduate Program, University of California, Riverside, CA 92521, USA

[2]Center for Nanotechnology and Nanotoxicology, Department of Environmental Health, Harvard T.H. Chan School of Public Health, Boston, MA 02115, USA

[3]Department of Chemistry, University of California, Riverside, CA 92521, USA

Abstract

In the presence of biological matrices, engineered nanomaterials, such as TiO₂, develop a biomolecular corona composed of lipids, proteins, etc. In this study, we analyzed the biocorona formed on the food grade TiO₂ (E171) going through an *in vitro* simulated gastrointestinal digestion system in either a fasting food model (FFM), a standardized food model (SFM), or a high fat food model (HFFM). Lipids and proteins were extracted from the biocorona and underwent untargeted lipidomic and label-free shotgun proteomic analyses. Our results showed that the biocorona composition was different before and after food digestion. After digestion, more diverse lipids were adsorbed compared to proteins, most of which were the enzymes added to the simulated digestion system. The corona lipid profile was distinct from the digested food model they presented in, although similarity in the lipid profiles between the corona and the food matrix increased with the fat content in the food model. The corona formed in the two low-fat environments of FFM and SFM shared a higher degree of similarity while very different from their corresponding matrix, with some lipid species adsorbed with high enrichment factors, indicating specific interaction with the TiO₂ surface outperforming lipid matrix concentration in determination of corona formation. Formation of the biocorona may have contributed to the reduced oxidative stress as well as toxicological impacts observed in cellular studies. The present work is the first to confirm persistent adsorption of biomolecules could occur on ingested

Conflicts of interest
There are no conflicts to declare.

Declaration of interests
The authors declare that they have no known competing financial interests or personal relationships that could have appeared to influence the work reported in this paper.

nanomaterials in food digestae. More future studies are needed to study the *in vivo* impacts of the biocorona, and shed lights on how the biocorona affects the biotransformations and fate of the ingested nanomaterials, which may impose impacts on human health.

Graphical Abstract
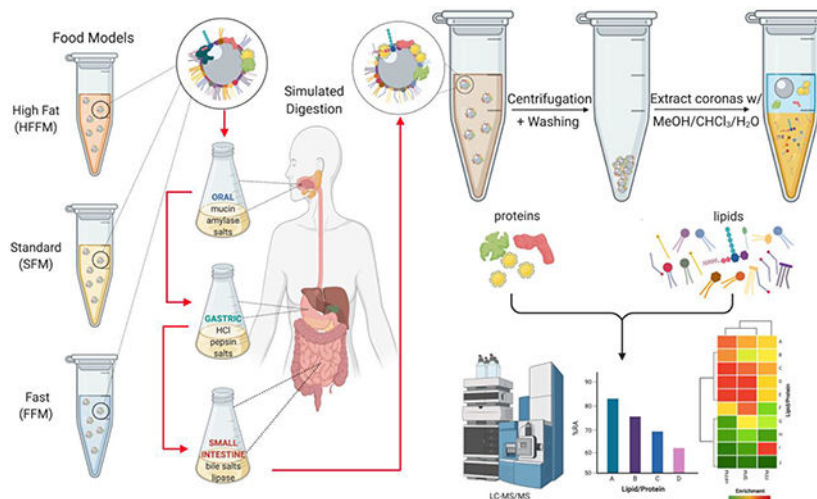
Keywords

biocorona; digested food model; lipidomics; proteomics; titanium dioxide nanoparticles

1. Introduction

Nanotechnology has the potential to revolutionize the agri-food industry, addressing issues related to agrichemical delivery, food quality, safety, and sustainability[1–4]. The smaller sizes of engineered nanomaterials (ENMs) gives them unique physicochemical and optoelectronic properties, which results in biointeractions differing substantially from those of the corresponding bulk materials[5–8]. Such biointeractions depend not only on the properties of the ENMs in the pristine form, but also on the agglomeration, dissolution, and particularly formation of biocoronas, during their contacts with the food matrix and the gastrointestinal tract (GIT)[6,9–14].

Adsorption of proteins, lipids and other molecules by ENMs from their surroundings result in biomolecular coronas that modulate the surface characteristics of ENMs[15–17], and in turn impacts the behavior of ENMs within complex biological systems[18,19], such as their distribution and cell/tissue responses[20–22]. Thus, studying the formation and composition of biocoronas could help to improve our understanding of the health impacts of ENMs. Several studies have investigated the formation of protein coronas on nanomaterials[12,23,24], including titanium dioxide (TiO_2)[25–27], after incubation with serum. Some have successfully identified soft and hard protein coronas[24,28,29] that are mainly different from each other in their binding affinity to the nanomaterial surface. Moreover, machine learning algorithms have been exploited to predict the protein corona composition on ENMs[12]. Besides the

protein corona, recent studies have also attempted to identify the lipid corona after incubation of ENMs in food matrices[30], serum[31], and plasma[32]. While our understanding of biocorona composition and its impact has expanded, there are a limited number of reports describing how the biocoronas on ingested ENMs change along with the process of digestion[33–35], which would be more relevant to their *in vivo* states and biointeractions during human exposure.

Food-grade TiO_2 (known as E171 in the European Union), is used as a pigment to increase whiteness and brightness in various food products, such as candies, pastries, and white sauces[36]. The estimated human exposure to TiO_2 through oral ingestion is about 1 mg per kilogram body weight per day for US adults and 1.4 – 10 fold higher for children under the age of ten[36]. Despite its wide application in the American diet, recent reports indicate that TiO_2 can be hazardous, with adverse effects including stimulation of intestinal and systemic inflammation, pathogenic changes in the gut microbiome composition[37,38], induction of oxidative stress in epithelial intestinal cells[39], preneoplastic lesion formation in the colon[40], epithelial-mesenchymal transition in intestinal epithelial cells[41] and exacerbation of colitis[42]. How TiO_2 interacts with the biological systems to induce such effects is not completely understood.

In the present work, we studied the biomolecular corona formed on food-grade TiO_2 (E171) during simulated three-phase (oral, gastric, and small intestinal) GIT digestion using three different food models. The lipid and protein compositions in the digested products (digestas) as well as the lipid and protein biocoronas on the surface of TiO_2 were identified and compared, revealing the highly enriched biomolecules on TiO_2 and the high dependence of the corona profile on the food matrix. Such information will help us to better understand the biointeractions of ingested ENMs along the GIT, and how such interactions would be different with varying diets.

2. Materials and Methods

2.1. Materials

Pristine food grade TiO_2, hereafter referred to as E171, was provided by the Engineered Nanomaterials Resource and Coordination Core (ERCC) at the Harvard T.H. Chan School of Public Health as part of the Nanotechnology Health Implications Research (NHIR) Consortium established by the National Institute of Environmental Health Sciences (NIEHS). Detailed physicochemical characterization of E171 was performed and described in detail by the authors in a previous publication[30]. The colloidal characterization of E171 following dispersion in various food models (see below) — obtained using a standardized dispersion method previously described by the authors[43] — has been documented by the authors[30,34,44]. A starting E171 concentration of 1% w/w in the food models was employed, following the permissible E171 concentrations in processed foods described in Title 21 of the Code of the Federal Regulations (21 CFR §73.575).

2.2. Food models

The fasting food model (FFM) consisted of 5 mM phosphate buffer at neutral pH (7.0). The standard food model (SFM), which is based on the average American diet, was formulated with 3.4% protein (sodium caseinate) and 3.4% fat (corn oil) as previously described by the authors[34,45]. Briefly, the SFM was created as an oil-in-water emulsion, spray dried for storage at 4°C, and reconstituted with distilled water. The high fat food model (HFFM), composed of approximately 3% protein and 13% fat, was prepared using heavy whipping cream purchased from a supermarket. The food models devoid of E171 were used as controls.

2.3. Characterization of E171 in different food models

Electron microscopy was performed at the Central Facility for Advanced Microscopy and Microanalysis at the UC Riverside. A droplet of the suspended sample was deposited onto a copper transmission electron microscopy (TEM) grid covered with a holey carbon support film, and allowed to dry in air. Conventional electron images were obtained in bright field mode on a FEI Co. Tecnai12 TEM operated at 120 kV accelerating voltage. Particles in suspension were counted with a Nanosight NS300 from Malvern Panalytical using a low volume flow cell chamber and a 405 nm laser module. Three video clips were collected, each for 30s, and processed with the Malvern nanoparticle tracking analysis (NTA) 3.3 software.

2.4. *In vitro* simulated digestions

The following samples were subjected to simulated digestion as previously described by the authors[10]: 1) FFM control, 2) FFM + 1% w/w TiO_2, 3) SFM control, 4) SFM control + 1% w/w TiO_2, 5) HFFM control, and 6) HFFM + 1% w/w TiO_2. Digestions were performed for each food model-ENM combination. Briefly, the simulated digestion consisted of an oral, gastric and small intestinal phase. In the oral phase the food model suspensions were warmed to 37 °C, combined with equal volumes of pre-warmed 37°C simulated saliva solution (containing salts, amylase, and mucin), and shaken by hand for 2 minutes to imitate chewing and mixing in the mouth. The resulting oral phase digestas were then diluted with equal volumes of simulated gastric fluid (containing HCl and additional salt) and incubated for 2 hours at 37°C in a shaking incubator at 200 rpm. Lastly, the gastric phase digestas were diluted by ~1/4 with simulated intestinal fluid (containing bile salts, pancreatic extract (containing amylase, lipase, and various proteases), and additional salts) and incubated at 37°C for 2 hours. Sample pH was kept at 7.0 using a pH Stat device (TitroLine® 7000, SI Analytics, GmbH, Germany). As a result of the combined dilutions during the oral, gastric, and small intestinal phases, the initial concentration of TiO_2 was diluted by a combined factor of ~1/12 before biomolecular extraction and analysis. Three biological repeats were performed.

2.5. Lipid extraction

Lipids from the control digestas, as well as the biocoronas from E171 in the different food models, were extracted using a modified Folch method[30]. Briefly, for each corona sample, a 15 mL aliquot was centrifuged at $10,000 \times g$ for 10 minutes to collect the nanoparticle pellet

and the supernatant containing the free lipids was removed. The pellet was washed twice by ultrapure water, with the supernatant removed each time following centrifugation; and then resuspended in 15 mL ultrapure water. The suspension was mixed with 5 mL chloroform and vortexed for 15 mins at 1300 rpm. The organic layer was collected and the lipids were desolvated with a SpeedVac concentrator (Savant, Irvine, CA, US). Immediately prior to analyzing the samples with MS, the lipid pellets were reconstituted at 5 μg/μL in chloroform: methanol: water (60:37.5:2.5, v/v/v) with 2.5 pmol/μL of the internal standard (1,2-diarachidoyl-sn-glycero-3-phosphocholine) added to correct for ionization efficiency. For the control digestas, 15 mL of each sample was introduced into a separatory funnel along with 15 mL of chloroform. The sample was agitated for 15 minutes with venting and the bottom organic layer was collected. This step was repeated twice to ensure maximal collection of lipids. The organic solvent was removed with SpeedVac concentration. The dried lipids were reconstituted as described above.

2.6. Protein extraction

Protein corona extraction started with precipitating the TiO_2 particles from 1 mL of the digested food sample by centrifugation at 16,000 ×g for 30 minutes at room temperature. The TiO_2 pellets were then washed with 100 μL of 1×PBS and re-centrifuged, and the supernatants were removed. The pellets were resuspended in 20 μL of 1×PBS and 100 μL of chloroform, followed by 15 minutes of agitation to remove the lipids from the corona. The aqueous layer, containing the TiO_2, was collected and diluted 1:1 with 2×Laemmli sample buffer (Bio-Rad, Hercules, CA, US). The proteins on the NP surfaces were then desorbed and denatured by heating the sample at 95°C for 5 minutes. One milliliter of each of the 3 digested food matrices, without TiO_2, were concentrated with PES 3K MWCO protein concentrators (Thermo Scientific™, US). After concentration, roughly 20 μL of the sample was collected and diluted with 80 μL of 1×PBS and 500 μL of chloroform. After the samples were agitated, the supernatant was collected and diluted with the 2×Laemmli sample buffer, and the proteins were desorbed as described above.

2.7. Gel electrophoresis

To visualize the desorbed corona proteins, as well as the denatured proteins from the controls, 15 μL of each mixture was separated by SDS-PAGE using a 12% polyacrylamide separation gel with 0.1% SDS, a 4% stacking gel, and 1× running buffer (Tris base, glycine and SDS) at a constant voltage of 180V for 55 minutes. The PageRuler Plus Prestained Protein Ladder (Fisher Scientific, Waltham, MA, US) was run as a molecular weight standard (10–250 kDa). Coomassie blue R-250 (Fisher Scientific) was utilized to stain protein bands. SDS-PAGE gels were imaged using a DSLR camera (Canon, San Jose, CA) and the resulting images were analyzed via ImageJ. The intensities of the band signals for the corona samples were normalized to the respective bands from the control samples.

2.8. Protein Digestion for Proteomics

One milliliter of each sample was subjected to protein precipitation following an adopted protocol[46]. Briefly, methanol, chloroform, and water were added to the controls followed by centrifugation at 14,000 × g for 5 minutes and removal of the aqueous layer. Methanol was reintroduced into each sample, followed by a quick vortex and centrifugation (14,000 × g, 5

minutes). The supernatant was removed, resulting in a protein flake that adhered to the wall of the tube. The sample was then dried via SpeedVac. For samples that contained nanoparticles, two washes with ultrapure water followed by centrifugations at $10,000 \times g$ for 10 minutes produced nanoparticle pellets with intact biocoronas. These samples were then subjected to the aforementioned protein precipitation.

Following precipitation of the protein, each sample was resuspended with 8 M urea in 50 mM ammonium bicarbonate. DTT was added at a final concentration of 5 mM and incubated for 40 minutes at 56°C. The sample was cooled to room temperature and exposed to 10 mM iodoacetamide in the dark for 45 minutes. The sample was diluted 8 times with 50 mM ammonium bicarbonate and trypsin was added in a mass ratio of 1:40 (trypsin:protein) to digest the proteins during overnight (16 hrs) incubation at 37°C. The samples that contained nanoparticles were then centrifuged at $15,000 \times g$ for 15 minutes to remove the nanomaterials. All samples were lyophilized, desalted, and resuspended in 0.1% formic acid for proteomic analysis.

2.9. LC-MS/MS proteomic analysis

Thermo nLC1200, in single-pump trapping mode, was used with a Thermo PepMap RSLC C18 EASY-spray column (2 μm, 100 Å, 75 μm x 25 cm) and a PepMap C18 trap column (3 μm, 100 Å, 75 μm x 20 cm) to perform liquid chromatography. Solvent A was water with 0.1% formic acid and solvent B was 80% acetonitrile with 0.1% formic acid. Samples were separated at 300 nL/min with a 250-minute gradient starting at 3% B, increasing to 30% B from 1–231 minutes, and then 85% B at 241 minutes, holding for 10 minutes.

Mass spectrometry was performed on a Thermo Orbitrap Fusion in a data-dependent mode. A full scan was conducted using 60k resolution in the Orbitrap in positive mode. Precursors for MS/MS were filtered by monoisotopic peak determination for peptides, intensity threshold 5.0e3, charge state 2–7, and 60 second dynamic exclusion after 1 analysis with a mass tolerance of 10 ppm. Higher energy C-trap dissociation (HCD) spectra were collected in ion trap MS/MS at 35% energy and isolation window 1.6 m/z.

2.10. Proteomic data processing

Data was searched individually in Proteome Discoverer 2.2 (Thermo Scientific, US) against the UniProt FASTA databases for *Bos Taurus* and *Sus Scrofa.* The precursors mass tolerance was set at up to 10 ppm and fragment mass tolerance to 0.6 Da. Fixed modifications were carbamidomethyl (Cys +57.021 Da), ^{13}C labelled carbamidomethyl (Cys +58.024 Da), and dynamic modifications included methionine oxidation (+15.995 Da) and N-terminal acetylation (+42.011 Da). Results were filtered to a strict 1% false discovery rate.

2.11. LC-MS lipidomic analysis

An untargeted lipidomics approach was employed at the UC Riverside Metabolomics Core Facility using a Waters UPLC system coupled to a Synapt G2-Si quadrupole time-of-flight MS. Separations were achieved on a CSH C18 column (Waters, 2.1× 100 mm, 1.7 μM) using gradient elution. Solvent A contained 60: 40 acetonitrile: water with 10 mM ammonium formate and 0.1% formic acid; and Solvent B was composed of 90: 10

isopropanol: acetonitrile with 10 mM ammonium formate and 0.1% formic acid. The gradient program was as follows: 0 min, 90% A; 1 min, 90% A; 3 min, 80% A; 5 min, 60% A; 16 min, 20% A; 18 min, 1% A; 20 min, 1 % A; 20.1 min, 90% A. The flow rate was 350 μL/min, the column was kept at 50° C and the injection volume was 1 μL. Source temperature was set at 150°C. Desolvation temperature and gas were set at 600°C and 1100 L/hr, respectively. Cone gas was set at 150L/hr. Apart from the collision gas (argon), all other gases utilized were nitrogen. Capillary voltage was 1 kV. Samples, run in positive ion mode (50–1200 m/z) with 100 ms scan time, were analyzed in duplicate and random order.

2.12. Lipidomic data processing

Data processing, including peak picking, alignment, deconvolution, integration, normalization, and spectral matching was performed in Progenesis Qi software (Nonlinear Dynamics). Data were normalized to total ion abundance. The data were searched against three mass spectral metabolite databases, including Metlin, Mass Bank of North America and an in-house database by the staff at the UC Riverside Metabolomics Core Facility.

2.13. Statistical analysis

For comparison of the lipid profiles in all samples, the relative abundance (RA) values of the identified lipids were calculated by normalizing the peak areas of each lipid, PA_i, to the peak area of the internal standard followed by calculating with Equation 1 for correction of running condition variations:

$$\%RA_i = \frac{normalized\ PA_i}{\Sigma normalized\ PA} \times 100\% \tag{1}$$

The same calculation was performed for proteins, except that the PA was replaced by the spectral count detected for each protein. RA values were then subjected to the Student's *t*-test to interpret p-values. The significance level was set at 5% and a false discovery rate approach was used.

To gain more information about how the food matrix has impacted the composition of the biocorona, we computed the %Similarity between food model controls and corresponding coronas for both lipid and protein composition among all samples using Equation 2:

$$\%Similarity = \frac{\sum \min(RA_a, RA_b)}{\sum \mathrm{avg}(RA_a, RA_b)} \times 100\% \tag{2}$$

All samples were prepared with three biological replicates and lipid analysis was repeated twice for each sample. Statistical analysis was performed using GraphPad Prism v8.4 and Excel. A two-way ANOVA with Tukey's multiple comparisons test or the two-tailed Student's *t*-test was applied for comparisons. *p*-values less than 0.05 were considered statistically significant. The clustered heatmaps were created using the heatmap3 package v1.1.7 ("complete" as the clustering method) in R v3.6.3. Principal component analysis (PCA) was performed using SIMCA v14.1.

3. Results

3.1. Composition of food matrix

Three food models were processed in the simulator with the presence of E171. Their simplified compositions before undergoing simulated digestion are summarized in Table S-1A. The FFM was composed of 5 mM phosphate buffer at biological pH with no lipid or protein in the food matrix. The SFM represented the average American diet, and contained variants of casein milk proteins (listed in Table S-1B) mixed homogenously with corn oil, which is known to be composed of triacylglycerides (TGs), sterols, phosphatidylcholines (PCs) and phosphatidylethanolamines (PEs)[47]. The HFFM mimicked the compositions in a high-fat diet, and was prepared by diluting the heavy cream purchased from a local grocery store. It had a similar relative quantity of total proteins as in the SFM, but more than 4 times more total lipids. In-depth analysis of the undigested SFM and HFFM by LC-MS/MS data revealed that in the undigested SFM, 90% of the lipids were TGs and 9% were diacylglycerides (DGs); while the HFFM was found to contain more than 85% TGs, 10% DGs, and 3% monoacylglycerols (MGs) (Figure S-3). Besides the original food components, during the simulated digestion process, enzymes mimicking those present in the GI tracks, such as proteases and lipases, were added (Table S-1B).

3.2. Characterization of E171 in the digestae

Detailed physicochemical characterization of E171 has been reported previously by the authors[30]. Briefly, XRD patterns revealed an anatase crystal form, with a mean particle size by TEM of 113.4 ± 37.2 nm, with approximately 40% particles having at least one dimension <100 nm, in agreement with what has been reported by others[36]. TEM images of E171 in the three digested food models are shown in Figure 1. The pristine E171 had a mean hydrodynamic diameter of 125.1 ± 6.6 nm when measured by NTA (Figure S-1) after being prepared with a standardized sonication protocol[43]. This pristine E171 exhibited no particle aggregation under TEM (Fig. 1A); but aggregated significantly in the food matrices. The aggregation phenomena agreed with what was reported in our previous work: the colloidal dimensions of E171 in the FFM and SFM after simulated digestion were above 10 μm using multi-angle laser diffraction (MALD)[34]. NTA measurement was attempted in the present work, but failed in measurement of the colloidal size of E171 in the food matrices due to the presence of a large number of background particles from the food matrices, and the aggregates being much larger than its measurement range. TEM images also illustrate a layer of halos around the E171 with lower contrast than the particles (Fig. 1B–D), which should be biocoronas. A thicker layer was seen on the particles prepared in the HFFM (Fig. 1D).

3.3. Lipidomic analysis of digested food models and coronas

To further study the composition of the biocorona, the lipids in the food digestae and the corresponding coronas were extracted by liquid-liquid extraction and subject for LC-MS/MS analysis. Figure S-2 displays the extracted lipid masses for each model and respective corona. Same amounts of total lipids were injected for all samples. A little more than 60 lipids were identified in all food models and their coronas, as listed in Table S-2. To gain an overview of the raw data before further processing, the original peak areas of the identified

lipids were analyzed with principal component analysis (PCA). The scores plot of the first principal component (depicted as t1) vs. the third PC (t3) (Figure S-4) showed that all analytical and biological repeats for each sample were included within the Hotelling's T^2 (95% confidence) ellipse, demonstrating a robust workflow and reproducible results. Substantial separation distances between different food models as well as their coronas were observed.

Since the original peak area could be affected by the running conditions of LC and the ionization efficiency in MS/MS, we normalized each peak area against that of the internal standard added to the sample, and used this normalized value to calculate the %RA, which represented the relative abundance of each lipid species in the sample. The bar plots of the %RA was displayed in Figure S-5, and pie charts were also constructed to illustrate the overall lipid profile in each sample, as shown in Figure 2. The lipids were grouped into 5 categories: glycerolipids (TGs, DGs, and MGs), glycerophospholipids (PC, lysoPCs, and lysoPE), sphingolipids (sphingomyelins (SMs) and ceramide), sterol lipids (bile acids, sterols, and cholesterol), and fatty acids (FA)[48]. For all lipid classes, statistical differences were found in their %RA between the corona and the matrix, with most having *p* values < 0.001, and in many cases < 0.0001. In particular, the corona from the SFM had 7.4× more DGs, 3.7× more lysoPCs, and 3.6× more SMs; but ~ 3× less bile acid and FAs than the matrix. The corona from the FFM contained 4.8× more sterols but 2.3× less bile acids (which were added during the small intestinal phase of the simulated digestion) than the matrix.

The Hierarchical Cluster Analysis (HCA) confirmed the visual comparison made on the pie charts: the matrices of FFM and SFM shared higher similarity with each other than with their respective corona samples; so did their coronas. To compare the lipid profiles more quantitatively, we calculated the %Similarity values among the samples (Figure 4). The lipid profiles for the coronas from SFM and FFM were quite similar (66%), so were those for the corresponding food matrices (61%), both higher than the similarity between the matrix and the corona, which was 39% and 47% for the FFM and the SFM, respectively. On contrary, the overall profiles of the matrix and the corona in the HFFM were similar between each other, sharing a high similarity of 74%. The lipid profile of the HFFM was dominated by the TG, DG, and MG species; and had only 29% and 17% similarities with the FFM and SFM controls, respectively.

To find out the lipids enriched in the corona, we also computed the fold change in the %RA of each lipid in the corona compared to that in the matrix, and plotted the $\log_2$ (fold change) ($\log_2(fc)$) values in Figure S-8 in the form of heatmaps, with the enriched lipids clustered by unsupervised hierarchical clustering. Statistical analysis on the $\log_2$ (fc) yielded a volcano (scatter) plot (Figure 5) that clearly revealed the lipids statistically enriched (green dots) or depleted (red dots) in the corona, with the cutoff $-\log_{10}$(p value) being 1.3. There were 26, 37, and 30 lipid significantly enriched in the coronas of the FFM, SFM, and HFFM, respectively (Table S-4), having $\log_2(fc)$ values > 0.5, i.e. fc > 1.5. We can also see the values of $\log_2(fc)$ have a wide range between 0 and 10 for the lipids found in the corona from the FFM, and this range becomes narrower, only up to 5, when the matrix changed to SFM, and the narrowest with the HFFM as the matrix. To compare the lipid enrichment

situations in the coronas among all food models, we constructed the Venn diagram on the statistically significant enriched lipids for each food model (Figure 6). Only 2 lipids (cholesterol and DG 36:3) were enriched on TiO_2 regardless of the food models. There were 16 lipids found in the coronas of both the FFM and SFM, 9 in the coronas of the SFM and HFFM, and 2 were found in the coronas of the FFM and HFFM.

3.4. Proteomic analysis of digested food models and coronas

Proteins in the food models and their corona were initially separated with SDS-PAGE to provide an overview of the protein composition in all samples (Figure S-6). Since most of the proteins should have been digested into peptides and even amino acids, we anticipated any whole proteins identified by this experiment were the enzymes added to the simulated digestion system (Table S-1). Very few proteins were recovered in the HFFM model and its corona, probably due to its high lipid content that impeded with protein extraction. For the SFM and FFM, obvious differences in band intensities were observed at roughly the 55 and 25–30 kDa positions between the food model controls and the coronas. The band densities at 55kDa, designated as the "protein A" group, were strong in both the FFM and the SFM, but diminished in the corresponding corona samples (Fig. S-6B). However, an opposite trend of change was observed in the "protein B/C" group at the range of 25–30 kDa (Fig. S-6C). This result indicates that adsorption of these two protein groups was reversely impacted by the presence of lipids.

To further identify the specific proteins in the food matrices and the coronas, the proteins were extracted (Fig. S-2 shows protein masses extracted), digested and analyzed with LC-MS/MS. Agreeing with our anticipation, more than 89% of the proteins identified in the digested food models and the corresponding corona samples were enzymes added for food digestion. Spectral counts were used for semi-quantification and for %RA calculation (Table S-3 & Figure S-7). Figure 3 shows the pie chart of the protein profile in each sample based on the %RA value of each protein. The protein profiles among all samples in general shared a higher %Similarity (all larger than 50%) than that of the lipid profiles. The higher lipid than protein contents in the digestas may have made the lipid species more dominant in the biocorona than the proteins, thus leading to the less distinct protein profiles among samples.

Trypsin was found the most abundant throughout all samples, but its proportion in the corona was higher than in the corresponding matrix. In contrast, α-amylase was the second abundant species in all food matrices, but only occupied a very small portion in the corona. These results agree with those from SDS-PAGE (Fig. S-6). Trypsin has a Mw ~ 24 kDa, and should belong to the "protein B/C" group, the band intensity of which was higher in the corona than in the matrix. The Mw of α-amylase is ~ 54 kDa, so it should belong to the "protein A" group on the gel, the band intensity of which decreased noticeably in the corona compared to in the matrix. Structural proteins, including collagen, fibrillin and laminin, were the second most abundant type of protein found across samples. These proteins likely originated from the bile extract used to digest the samples[49].

We also calculated the $\log_2$(fc) values for the proteins identified in all samples, and analyzed them statistically, with the volcano plot is displayed in Fig. 5 and heatmap in Figure S-9. All of the proteins showing large changes in the %RA values between the matrix and corona are

listed in Table S-5. Although 16, 13, and 20 proteins were found with the $\log_2(fc)$ ranging from −5 to 15 in the FFM, SFM, and HFFM corona, respectively, only 1 or 2 corona proteins were significantly enriched in each food model. They are trypsin and peptidase S1 domain-containing protein in the FFM; chymotrypsin c precursor in the SFM; and triacylglycerol lipase and chymotrypsin-like elastase family member 1 in the HFFM. The corona from the FFM enriched putative trypsinogen and triacylglycerol lipase while that in the HFFM had significantly more cytosolic lipocalin protein and the α-1 chain of type I collagen than the matrix (i.e. %RA increased significantly). Moreover, the corona from the SFM enriched triacylglycerol lipase. Interestingly, all the coronas, regardless of the food matrix, enriched the peptidase S1 domain-containing protein, triacylglycerol lipase, and trypsin.

4. Discussion

Biocoronas can affect the biological responses to ingested ENMs, such as food-grade TiO_2 (E171)[5], and should be studied as part of the toxicological assessment. While it has been well recognized that biocorona formation is a highly dynamic process, changing along with the surrounding environment, most reports focus on corona formation in static matrices, with few looking at the composition of the biomolecular corona during biological transformation[50]. Owing to the establishment of a gastrointestinal simulator in our lab, we were able to look at the biocorona formed on the TiO_2 as a function of the food matrix while going through the digestion process, which can better mimic the *in vivo* situation than simply looking at the undigested food models as we and others did previously[30]. To our understanding, there have been no other reports that have investigated the biocorona composition on food-grade TiO_2 (E171) after simulated digestion as a function of food matrix. Foods processed in this simulated digestion system, in addition to the selection of three different food models that are representative of American diets, are well suited for studies that aim to learn about how the food matrix changes during digestion could impact both the lipid and protein corona formation and thus, the biological properties of the material.

Layers of biocorona were observed around the E171 in the TEM images, with that around the particles in the HFFM being the thickest. This was confirmed by the good amounts of lipids recovered from the E171 and indeed, the lipid mass extracted from the HFFM corona was the highest among the samples prepared in these three food matrices (Fig. S-2). The large lipid mass recovered from the particles also hints that, multiple layers of lipids could be formed on the particle surface, which may have mediated more particle-particle interaction due to the high hydrophobicity of the lipids, and induced extensive particle aggregation observed in Fig. 1D.

Analysis of the corona composition revealed the strong impacts from the matrix components to the biocorona composition. One evidence is that, the corona composition changes along with the digestion process. Lipidomic analysis of the undigested SFM and HFFM controls showed that these were comprised of approximately 90% and 85% TGs (Fig. S-3). The present study revealed that, following digestion, there was an 80% reduction of TGs in the SFM and a 25% reduction in HFFM, which were broken down into simpler species, such as

DGs and MGs. Corresponding to the changes of the matrix composition after digestion, the corona profiles formed in the undigested and digested food models were different. For example, there was a 3-fold increase of DG species after digestion as well as a 22% decrease in TGs in the corona of HFFM, and the corona formed in the SFM had a reduction of 58% TGs after digestion, agreeing with the changes in their relative contents before and after digestion.

In addition, corona profiles, in particular, the lipid profiles, are different among the three digested food models, although those formed in FFM and SFM exhibited higher similarity than with that formed in HFFM. The lipid corona formed in HFFM had a high %Similarity (74%) with its matrix (Fig. 2 & 4). The HFFM contained a higher lipid content than the SFM and FFM, which led to a higher amount of lipids recovered from the E171 (Fig. S2). The high amount of lipid found in the corona of the E171 present in HFFM indicates, multiple layers of lipid adsorption could have occurred. Adsorption of the multiple biomolecule layers on NPs in different matrices has been widely reported in the study of protein corona[15], termed hard and soft coronas[24]. The inner layer of the corona (i.e.: the hard corona) could be lipids that interact directly with E171 via hydrogen bonding between the lipids' hydroxyl groups and the protruding oxygen on the NP surface. Such interactions should be more selective, and dependent on lipid concentration to a low extent. However, this hard corona could initiate adsorption of multiple outer layers (i.e.: soft corona) via hydrophobic interactions between lipids: lipids are highly hydrophobic and could be squeezed out of the aqueous environment in the food model solutions to adhere to the solid surface of E171[57]. Lipids at higher concentrations in the matrix should be adsorbed more, yielding a high similarity between the lipid profiles of the matrix and the corona.

In contrast, the FFM and SFM have lower lipid concentrations than the HFFM, possibly leading to less concentration-dependent lipid adsorption. Indeed, the FFM and SFM coronas carried low similarity with their corresponding matrix, which is opposite to the situation observed in the HFFM. The lipids found in the coronas of FFM and SFM (Table S-4) exhibited much higher $\log_2(fc)$ values than those in the HFFM: for the corona lipids in the SFM and FFM the maximum $\log_2(fc)$ was 9.6 and 4.4, respectively, with that for the HFFM being only 2.8. Several lyso PC, DG, and SM species, like lysoPC 18:0, DG 36:3, and SM 42:1 were highly enriched in the coronas of the SFM and the FFM. These species could be adsorbed owing to their specific interaction with the TiO_2 surface. Theoretically, pristine TiO_2 materials should have oxygen and Ti protruding from their surface and should therefore form hydrated structures in aqueous suspensions[51,52]. The hydroxyl groups of the glycerol backbone of DG and lysoPC can interact with O on the surface of TiO_2 through H-bonding[53]. Such interactions could also occur to SMs that has a sphingosine with a hydroxyl functional group[54,55]. SM also consists of a phosphocholine and a fatty acid moiety that has a phosphate and a carboxylic group, respectively, which can coordinate with Ti on the surface of the E171[56]. An interesting fact shown in Fig. 2 is that, the proportion of DGs in the coronas formed in both the FFM and SFM increased compared to the matrix controls, while that of bile acids decreased to a large extent. We speculate that, since TiO_2 can coordinate with OH^- in neutral pH solutions[58], the negatively charged bile acids could be repelled from the surface of E171. Besides, TiO_2 can have moderate hydrophobicity[59] which may also attribute to the higher proportion of neutral sterols than acidic bile sterols in the

corona. Selective inclusion of matrix lipid components has also been reported previously[31], which observed the selective adhesion of TGs and sterols to the polystyrene particles after incubation in serum.

The extent and composition of lipid coronas on the TiO_2 present in the food digestae revealed in this work may help explain their cellular impacts found in our *in vitro* study reported previously[34,45]. We found that, the E171 incubated in the SFM induced slightly lower cytotoxicity in the triculture gut epithelium cellular model than that in the FFM, which could be due to the formation of the biocorona revealed in the present work. Still, significantly high ROS production was observed[34]. This is not surprising, because the food-grade E171 is anatase TiO_2, which has high photocatalytic activity[60], and can generate hydroxyl radicals with or without UV radiation[53,61,62]. As we discussed above, the enriched species in the coronas from SFM and FFM could be adsorbed via H-bonding between the O of TiO_2 and hydroxyl or carboxyl groups on the lipids. Such interactions have been reported to lead to dissociative adsorption and potentially expose the active particle surface to cause ROS production[63].

The potential of anatase TiO_2 in radical generation may enhance oxidation of the lipids adsorbed on the particles, which in turn could trigger oxidative responses in cells upon exposure to TiO_2[27,39]. Indeed, in the corona formed in FFM, we observed 14.1× more saturated lysoPCs and 1.2× more saturated TGs compared to unsaturated lipids. The FFM contained no food lipid or protein except for the biomolecules originally present in the simulated GIT digestion system, leading to a simple and likely very thin corona formed on the TiO_2 surface. The active surface uncovered then may have caused more unsaturated lipids to be oxidized. The oxidized species in the corona of FFM may have contributed to the cellular oxidative stress observed in Cao *et al.*'s previous findings when cells were exposed to the TiO_2 in the FFM[34].

However, the trend of lipid oxidation in the coronas formed in the SFM and HFFM was the opposite of that in the FFM: the corona formed in these two matrices contained more unsaturated lipids than saturated ones, and the proportion was higher than that observed in the matrix. For example, the corona formed in the SFM had 28.9× more unsaturated DGs than saturated DGs, as well as 1.8× more unsaturated TGs than saturated TGs.; while the SFM control had only 0.9× more unsaturated DGs than saturated DGs and 1.2× more unsaturated TGs than saturated TGs. In the case of HFFM, the corona had a large abundance of unsaturated DGs, and 3.3× more unsaturated TGs than saturated TGs; while the HFFM control had 3.2× more saturated DGs than unsaturated DGs and 1.6× more unsaturated TGs than saturated TGs. Since more lipids were found in the coronas of SFM and HFFM than in that from FFM, they could have covered up the reactive sites and reduced radical formation. Then the higher abundance of the unsaturated lipids in the corona than their saturated counterparts may be due to their capability in soliciting stronger induced dipole interaction[64] when binding to the surface of TiO_2 as well as to other lipids that facilitate the formation of multiple corona layers. On the other hand, the large numbers of unsaturated lipids found in the corona and the food matrix of SFM, may have activated the expression of cellular machinery involved in prevention of lipid peroxidation, like GPX4 and mitochondrial methylmalonate-semialdehyde (MMSA) dehydrogenase. GPX4 is a phospholipid

hydroperoxide glutathione peroxidase[65] that protects cells against membrane lipid peroxidation by directly reducing phospholipid hydroperoxide[66], and MMSA is involved in redox processes[67]. They were both found upregulated in cells treated with the SFM; and treatment with SFM + TiO$_2$ digestas induced even higher expression[34]. More detailed studies on lipid oxidation in the corona of reactive ENMs should be conducted to confirm our observations made in this work and dissect their impacts *in vitro*.

We found both lipids and proteins in the biocorona of E171 present in the food matrices. The total mass of proteins recovered from the particles was lower than that of lipids (Fig. S-2): the lipid masses extracted from the controls were 58 ×, 128 × and 141 × larger than the protein masses extracted from the FFM, SFM, and HFFM, respectively. For the corresponding coronas, there were 51 ×, 81 ×, and 99 × more lipids than proteins extracted. The relatively low abundance of extracted proteins from both the matrices and coronas are a result of the majority of the food proteins going through complete digestion. Concomitantly the total number of proteins identified by MS was lower than that of the lipids. The majority of proteins that remain intact within the food models and the corresponding corona samples are the enzymes that were added during the simulated digestion, although no proteins were found enriched on the corona across the different food models (Fig. 6). Adsorption of these enzymes could be through the charged amino acid residues, such as Arginine (Arg), Lysine (Lys), Glutamic acid (Glu) and Aspartic acid (Asp), which have been found to have strong affinity to TiO$_2$[68]. It is worth noting that, several of them, including α-amylase, phospholipase A2, and chymotrypsin c, have Asp residues in their active sites. If adsorption on TiO$_2$ is mediated partially by the Asp residue in the active site, the function of the protein could be strongly affected. It has been shown that TiO$_2$ nanoparticles are able to decrease the extent of gastric digestion of dietary protein casein[14]. Further studies are necessary to confirm the binding sites of these enzymatic proteins to the surfaces of TiO$_2$ as well as the function of these after interaction with the nanomaterial.

In addition, the difference in the protein compositions between the matrix and corona observed among all three food models indicate that, the lipid and protein components could affect one another for inclusion in the corona. For instance, α-amylase (Mw ~ 51–54 kDa) was highly abundant in the food model controls, but its %RA dropped as the lipid contents in the matrix increased. On the contrary, trypsin and chymotrypsin, which have Mw ~25–35 kDa, in the corona of the SFM was lower than those in the FFM. Although this study did not assay the competitive binding of these biomolecules, the observations in %RA hint that lipid adsorption could have competed these proteins off the surface of TiO$_2$. These are interesting aspects worthy of future exploration.

5. Conclusion

This study reports the composition of both the lipid and protein corona formed on the surfaces of the food-grade TiO$_2$ (E171) present in simulated digestae of three food models. The results demonstrate that, the biocorona formed on the surface of the food-borne nanoparticles would evolve during the process of digestion, and be strongly impacted by the matrix composition. In the HFFM with high fat contents, the corona composition was very similar to that of the matrix; but the corona formed in the SFM or FFM containing much less

fat, had very distinct composition than its matrix, and some lipids were highly enriched. These lipids all contain functional groups with high affinity to TiO_2. Although lipids dominated the biocorona, and even depleted some proteins from the corona, significant enrichment of few digestion enzymes was revealed. Formation of the biocorona could passivate the surface of TiO_2, reducing cellular toxicity of the particles. On the other hand, the adsorbed lipids may be oxidized by the radicals generated by the TiO_2. More studies on whether the functions of the adsorbed enzymes could be affected, as well as whether the adsorbed biomolecules could react with the particle surface should be conducted in the future to fully dissect the potential impacts on the corona molecules, which could in turn contribute to the biological impacts from the particles. Additionally, the methods utilized in this work can be expanded to study the corona formation on other nanomaterials in different biological matrices. Subsequent investigations will bridge together multiple facets of the bio-nano interface and toxicology to develop safer consumable food grade nanomaterials.

Supplementary Material

Refer to Web version on PubMed Central for supplementary material.

Acknowledgments

References

(1). Deloid GM; Sohal IS; Lorente LR; Molina RM; Pyrgiotakis G; Stevanovic A; Zhang R; McClements DJ; Geitner NK; Bousfield DW; et al. Reducing Intestinal Digestion and Absorption of Fat Using a Nature-Derived Biopolymer: Interference of Triglyceride Hydrolysis by Nanocellulose. ACS Nano 2018, 12 (7), 6469–6479. 10.1021/acsnano.8b03074. [PubMed: 29874029]

(2). Vaze N; Pyrgiotakis G; Mena L; Baumann R; Demokritou A; Ericsson M; Zhang Y; Bello D; Eleftheriadou M; Demokritou P A Nano-Carrier Platform for the Targeted Delivery of Nature-Inspired Antimicrobials Using Engineered Water Nanostructures for Food Safety Applications. Food Control 2019, 96 (8 2018), 365–374. 10.1016/j.foodcont.2018.09.037.

(3). Eleftheriadou M; Pyrgiotakis G; Demokritou P Nanotechnology to the Rescue: Using Nano-Enabled Approaches in Microbiological Food Safety and Quality. Curr. Opin. Biotechnol 2017, 44, 87–93. 10.1016/j.copbio.2016.11.012. [PubMed: 27992831]

(4). Rodrigues SM; Demokritou P; Dokoozlian N; Hendren CO; Karn B; Mauter MS; Sadik OA; Safarpour M; Unrine JM; Viers J; et al. Nanotechnology for Sustainable Food Production: Promising Opportunities and Scientific Challenges. Environ. Sci. Nano 2017, 4 (4), 767–781. 10.1039/c6en00573j.

(5). McClements DJ; Xiao H Is Nano Safe in Foods? Establishing the Factors Impacting the Gastrointestinal Fate and Toxicity of Organic and Inorganic Food-Grade Nanoparticles. npj Sci. Food 2017, 1 (1), 6 10.1038/s41538-017-0005-1. [PubMed: 31304248]

(6). Sohal IS; O'Fallon KS; Gaines P; Demokritou P; Bello D Ingested Engineered Nanomaterials: State of Science in Nanotoxicity Testing and Future Research Needs. Part. Fibre Toxicol 2018, 15 (1). 10.1186/s12989-018-0265-1.

(7). Grassian VH; Haes AJ; Mudunkotuwa IA; Demokritou P; Kane AB; Murphy CJ; Hutchison JE; Isaacs JA; Jun YS; Karn B; et al. NanoEHS - Defining Fundamental Science Needs: No Easy Feat When the Simple Itself Is Complex. Environ. Sci. Nano 2016, 3 (1), 15–27. 10.1039/c5en00112a.

(8). Parviz D; Bitounis D; Demokritou P; Strano M Engineering Two-Dimensional Nanomaterials to Enable Structure-Activity Relationship Studies in Nanosafety Research. NanoImpact 2020, 18 (4), 100226 10.1016/j.impact.2020.100226. [PubMed: 32617436]

(9). Sohal IS; Cho YK; O'Fallon KS; Gaines P; Demokritou P; Bello D Dissolution Behavior and Biodurability of Ingested Engineered Nanomaterials in the Gastrointestinal Environment. ACS Nano 2018, 12 (8), 8115–8128. 10.1021/acsnano.8b02978. [PubMed: 30021067]

(10). DeLoid GM; Wang Y; Kapronezai K; Lorente LR; Zhang R; Pyrgiotakis G; Konduru NV; Ericsson M; White JC; De La Torre-Roche R; et al. An Integrated Methodology for Assessing the Impact of Food Matrix and Gastrointestinal Effects on the Biokinetics and Cellular Toxicity of Ingested Engineered Nanomaterials. Part. Fibre Toxicol 2017, 14 (1), 1–17. 10.1186/s12989-017-0221-5. [PubMed: 28069023]

(11). McClements DJ; DeLoid G; Pyrgiotakis G; Shatkin JA; Xiao H; Demokritou P The Role of the Food Matrix and Gastrointestinal Tract in the Assessment of Biological Properties of Ingested Engineered Nanomaterials (IENMs): State of the Science and Knowledge Gaps. NanoImpact 2016, 3–4, 47–57. 10.1016/j.impact.2016.10.002.

(12). Duan Y; Coreas R; Liu Y; Bitounis D; Zhang Z; Parviz D; Strano MS; Demokritou P; Zhong W Prediction of Protein Corona on Nanomaterials by Machine Learning Using Novel Descriptors; 2019.

(13). Konduru NV; Molina RM; Swami A; Damiani F; Pyrgiotakis G; Lin P; Andreozzi P; Donaghey TC; Demokritou P; Krol S; et al. Protein Corona: Implications for Nanoparticle Interactions with Pulmonary Cells. Part. Fibre Toxicol 2017, 14 (1), 1–12. 10.1186/s12989-017-0223-3. [PubMed: 28069023]

(14). Cao X; Han Y; Li F; Li Z; McClements DJ; He L; Decker EA; Xing B; Xiao H Impact of Protein-Nanoparticle Interactions on Gastrointestinal Fate of Ingested Nanoparticles: Not Just Simple Protein Corona Effects. NanoImpact 2019, 13 (11 2018), 37–43. 10.1016/j.impact.2018.12.002.

(15). Nel AE; Mädler L; Velegol D; Xia T; Hoek EMV; Somasundaran P; Klaessig F; Castranova V; Thompson M Understanding Biophysicochemical Interactions at the Nano-Bio Interface. Nat. Mater 2009, 8 (7), 543–557. 10.1038/nmat2442. [PubMed: 19525947]

(16). Maiorano G; Sabella S; Sorce B; Brunetti V; Malvindi MA; Cingolani R; Pompa PP Effects of Cell Culture Media on the Dynamic Formation of Protein-Nanoparticle Complexes and Influence on the Cellular Response. ACS Nano 2010, 4 (12), 7481–7491. 10.1021/nn101557e. [PubMed: 21082814]

(17). Duan Y; Liu Y; Coreas R; Zhong W Mapping Molecular Structure of Protein Locating on Nanoparticles with Limited Proteolysis. Anal. Chem 2019, 91, acs.analchem.9b00482. 10.1021/acs.analchem.9b00482.

(18). Clift MJD; Bhattacharjee S; Brown DM; Stone V The Effects of Serum on the Toxicity of Manufactured Nanoparticles. Toxicol. Lett 2010, 198 (3), 358–365. 10.1016/j.toxlet.2010.08.002. [PubMed: 20705123]

(19). Yin H; Chen R; Casey PS; Ke PC; Davis TP; Chen C Reducing the Cytotoxicity of ZnO Nanoparticles by a Pre-Formed Protein Corona in a Supplemented Cell Culture Medium. RSC Adv. 2015, 5 (90), 73963–73973. 10.1039/c5ra14870g.

(20). Abbina S; Takeuchi LE; Anilkumar P; Yu K; Rogalski JC; Shenoi RA; Constantinescu I; Kizhakkedathu JN Blood Circulation of Soft Nanomaterials Is Governed by Dynamic Remodeling of Protein Opsonins at Nano-Biointerface. Nat. Commun 2020, No. 2020, 1–12. 10.1038/s41467-020-16772-x. [PubMed: 31911652]

(21). Bertrand N; Grenier P; Mahmoudi M; Lima EM; Appel EA; Dormont F; Lim JM; Karnik R; Langer R; Farokhzad OC Mechanistic Understanding of in Vivo Protein Corona Formation on

Polymeric Nanoparticles and Impact on Pharmacokinetics. Nat. Commun 2017, 8 (1). 10.1038/s41467-017-00600-w.

(22). Liu N; Tang M; Ding J The Interaction between Nanoparticles-Protein Corona Complex and Cells and Its Toxic Effect on Cells. Chemosphere 2020 10.1016/j.chemosphere.2019.125624.

(23). Lara S; Alnasser F; Polo E; Garry D; Lo Giudice MC; Hristov DR; Rocks L; Salvati A; Yan Y; Dawson KA Identification of Receptor Binding to the Biomolecular Corona of Nanoparticles. ACS Nano 2017, 11 (2), 1884–1893. 10.1021/acsnano.6b07933. [PubMed: 28112950]

(24). Ashby J; Pan S; Zhong W Size and Surface Functionalization of Iron Oxide Nanoparticles Influence the Composition and Dynamic Nature of Their Protein Corona. ACS Appl. Mater. Interfaces 2014, 6 (17), 15412–15419. 10.1021/am503909q. [PubMed: 25144382]

(25). Gunnarsson SB; Bernfur K; Mikkelsen A; Cedervall T Analysis of Nanoparticle Biomolecule Complexes. Nanoscale 2018, 10 (9), 4246–4257. 10.1039/c7nr08696b. [PubMed: 29436548]

(26). Proquin H; Rodríguez-Ibarra C; Moonen CGJ; Urrutia Ortega IM; Briedé JJ; de Kok TM; van Loveren H; Chirino YI Titanium Dioxide Food Additive (E171) Induces ROS Formation and Genotoxicity: Contribution of Micro and Nano-Sized Fractions. Mutagenesis 2017, 32 (1), 139–149. 10.1093/mutage/gew051. [PubMed: 27789654]

(27). Jayaram DT; Runa S; Kemp ML; Payne CK Nanoparticle-Induced Oxidation of Corona Proteins Initiates an Oxidative Stress Response in Cells. Nanoscale 2017, 9 (22), 7595–7601. 10.1039/C6NR09500C. [PubMed: 28537609]

(28). Milani S; Baldelli Bombelli F; Pitek AS; Dawson KA; Rädler J Reversible versus Irreversible Binding of Transferrin to Polystyrene Nanoparticles: Soft and Hard Corona. ACS Nano 2012, 6 (3), 2532–2541. 10.1021/nn204951s. [PubMed: 22356488]

(29). Cedervall T; Lynch I; Lindman S; Berggard T; Thulin E; Nilsson H; Dawson K a; Linse, S. Understanding the Nanoparticle-Protein Corona Using Methods to Quantify Exchange Rates and Affinities of Proteins for Nanoparticles. Proc. Natl. Acad. Sci 2007, 104 (7), 2050–2055. 10.1073/pnas.0608582104. [PubMed: 17267609]

(30). Lee JY; Wang H; Pyrgiotakis G; DeLoid GM; Zhang Z; Beltran-Huarac J; Demokritou P; Zhong W Analysis of Lipid Adsorption on Nanoparticles by Nanoflow Liquid Chromatography-Tandem Mass Spectrometry. Analytical and Bioanalytical Chemistry. 2018 10.1007/s00216-018-1145-0.

(31). Lima T; Bernfur K; Vilanova M; Cedervall T Understanding the Lipid and Protein Corona Formation on Different Sized Polymeric Nanoparticles. Sci. Rep 2020, 10 (1), 1129 10.1038/s41598-020-57943-6. [PubMed: 31980686]

(32). La Barbera G; Capriotti AL; Caracciolo G; Cavaliere C; Cerrato A; Montone CM; Piovesana S; Pozzi D; Quagliarini E; Laganà A A Comprehensive Analysis of Liposomal Biomolecular Corona upon Human Plasma Incubation: The Evolution towards the Lipid Corona. Talanta 2019 10.1016/j.talanta.2019.120487.

(33). Sieg H; Kästner C; Krause B; Meyer T; Burel A; Böhmert L; Lichtenstein D; Jungnickel H; Tentschert J; Laux P; et al. Impact of an Artificial Digestion Procedure on Aluminum-Containing Nanomaterials. Langmuir 2017, 33 (40), 10726–10735. 10.1021/acs.langmuir.7b02729. [PubMed: 28903564]

(34). Cao X; Zhang T; DeLoid GM; Gaffrey M; Weitz K; Thrall B; Qian WJ; Demokritou P Evaluation of the Cytotoxic and Cellular Proteome Impacts Offood- Grade TiO2 (E171) Using Simulated Gastrointestinal Digestions and a Tri-Culture Small Intestinal Epithelial Model. NanoImpact 2019 10.1016/j.impact.2019.100202.

(35). DeLoid GM; Cao X; Molina RM; Silva DI; Bhattacharya K; Ng KW; Loo SCJ; Brain JD; Demokritou P Toxicological Effects of Ingested Nanocellulose in in Vitro Intestinal Epithelium and in Vivo Rat Models. Environ. Sci. Nano 2019, 2105–2115. 10.1039/c9en00184k. [PubMed: 32133146]

(36). Weir A; Westerhoff P; Fabricius L; Hristovski K; Von Goetz N Titanium Dioxide Nanoparticles in Food and Personal Care Products. Environ. Sci. Technol 2012, 46 (4), 2242–2250. 10.1021/es204168d. [PubMed: 22260395]

(37). Mu W; Wang Y; Huang C; Fu Y; Li J; Wang H; Jia X; Ba Q Effect of Long-Term Intake of Dietary Titanium Dioxide Nanoparticles on Intestine Inflammation in Mice. J. Agric. Food Chem 2019, 67 (33), 9382–9389. 10.1021/acs.jafc.9b02391. [PubMed: 31361959]

(38). Cao X; Han Y; Gu M; Du H; Song M; Zhu X; Ma G; Pan C; Wang W; Zhao E; et al. Foodborne Titanium Dioxide Nanoparticles Induce Stronger Adverse Effects in Obese Mice than Non-Obese Mice: Gut Microbiota Dysbiosis, Colonic Inflammation, and Proteome Alterations. Small 2020, 2001858, 1–16. 10.1002/smll.202001858.

(39). Dorier M; Béal D; Marie-Desvergne C; Dubosson M; Barreau F; Houdeau E; Herlin-Boime N; Carriere M Continuous in Vitro Exposure of Intestinal Epithelial Cells to E171 Food Additive Causes Oxidative Stress, Inducing Oxidation of DNA Bases but No Endoplasmic Reticulum Stress. Nanotoxicology 2017, 11 (6), 751–761. 10.1080/17435390.2017.1349203. [PubMed: 28671030]

(40). Bettini S; Boutet-Robinet E; Cartier C; Coméra C; Gaultier E; Dupuy J; Naud N; Taché S; Grysan P; Reguer S; et al. Food-Grade TiO 2 Impairs Intestinal and Systemic Immune Homeostasis, Initiates Preneoplastic Lesions and Promotes Aberrant Crypt Development in the Rat Colon. Sci. Rep. 2017, 7 (12 2016), 1–13. 10.1038/srep40373.

(41). Setyawati MI; Sevencan C; Bay BH; Xie J; Zhang Y; Demokritou P; Leong DT Nano-TiO2 Drives Epithelial–Mesenchymal Transition in Intestinal Epithelial Cancer Cells. Small 2018, 14 (30), 1–13. 10.1002/smll.201800922.

(42). Ruiz PA; Morón B; Becker HM; Lang S; Atrott K; Spalinger MR; Scharl M; Wojtal KA; Fischbeck-Terhalle A; Frey-Wagner I; et al. Titanium Dioxide Nanoparticles Exacerbate DSS-Induced Colitis: Role of the NLRP3 Inflammasome. Gut 2017, 66 (7), 1216–1224. 10.1136/gutjnl-2015-310297. [PubMed: 26848183]

(43). DeLoid GM; Cohen JM; Pyrgiotakis G; Demokritou P Preparation, Characterization, and in Vitro Dosimetry of Dispersed, Engineered Nanomaterials. Nat. Protoc 2017, 12 (2), 355–371. 10.1038/nprot.2016.172. [PubMed: 28102836]

(44). Cao X; DeLoid G; Bitounis D; De La Torre R; White J; Zhang Z; Ho CG; Ng KW; Eitzer B; Demokritou P Co-Exposure to the Food Additives SiO2 (E551) or TiO2 (E171) and the Pesticide Boscalid Increases Cytotoxicity and Bioavailability of the Pesticide in a Tri-Culture Small Intestinal Epithelium Model: Potential Health Implications. Environ. Sci. Nano 2019 10.1039/C9EN00676A.

(45). Zhang Z; Zhang R; Xiao H; Bhattacharya K; Bitounis D; Demokritou P; McClements DJ Development of a Standardized Food Model for Studying the Impact of Food Matrix Effects on the Gastrointestinal Fate and Toxicity of Ingested Nanomaterials. NanoImpact 2019, 13 (11 2018), 13–25. 10.1016/j.impact.2018.11.002.

(46). Wessel D; Flügge UI A Method for the Quantitative Recovery of Protein in Dilute Solution in the Presence of Detergents and Lipids. Anal. Biochem 1984, 138 (1), 141–143. 10.1016/0003-2697(84)90782-6. [PubMed: 6731838]

(47). Moreau RA; Powell MJ; Singh V Pressurized Liquid Extraction of Polar and Nonpolar Lipids in Corn and Oats with Hexane, Methylene Chloride, Isopropanol, and Ethanol. JAOCS, J. Am. Oil Chem. Soc 2003, 80 (11), 1063–1067. 10.1007/s11746-003-0821-y.

(48). Fahy E; Subramaniam S; Brown HA; Glass CK; Merrill AH; Murphy RC; Raetz CRH; Russell DW; Seyama Y; Shaw W; et al. A Comprehensive Classification System for Lipids. J. Lipid Res 2005, 46 (5), 839–861. 10.1194/jlr.E400004-JLR200. [PubMed: 15722563]

(49). Juvonen T; Kairaluoma MI; Malinen H; Niemelä O Extracellular Matrix Proteins in Bile and Serum of Patients with Gallstone Disease. Connect. Tissue Res 1993, 29 (3), 171–180. 10.3109/03008209309016824. [PubMed: 8222644]

(50). Walczak AP; Kramer E; Hendriksen PJM; Helsdingen R; Van Der Zande M; Rietjens IMCM; Bouwmeester H In Vitro Gastrointestinal Digestion Increases the Translocation of Polystyrene Nanoparticles in an in Vitro Intestinal Co-Culture Model. Nanotoxicology 2015, 9 (7), 886–894. 10.3109/17435390.2014.988664. [PubMed: 25672814]

(51). Wang CY; Groenzin H; Shultz MJ Molecular Species on Nanoparticulate Anatase TiO2 Film Detected by Sum Frequency Generation: Trace Hydrocarbons and Hydroxyl Groups. Langmuir 2003, 19 (18), 7330–7334. 10.1021/la0345542.

(52). Diebold U The Surface Science of Titanium Dioxide. Surf. Sci. Rep 2002, 48 (1), 53–229. 10.1016/S0167-5729(02)00100-0.

(53). Zhang J; Nosaka Y Mechanism of the OH Radical Generation in Photocatalysis with TiO 2 of Different Crystalline Types. J. Phys. Chem. C 2014, 118 (20), 10824–10832. 10.1021/jp501214m.

(54). Wendt S; Schaub R; Matthiesen J; Vestergaard EK; Wahlström E; Rasmussen MD; Thostrup P; Molina LM; Lægsgaard E; Stensgaard I; et al. Oxygen Vacancies on TiO2(1 1 0) and Their Interaction with H2O and O2: A Combined High-Resolution STM and DFT Study. Surf. Sci 2005, 598 (1–3), 226–245. 10.1016/j.susc.2005.08.041.

(55). Pan X; Yang MQ; Fu X; Zhang N; Xu YJ Defective TiO2 with Oxygen Vacancies: Synthesis, Properties and Photocatalytic Applications. Nanoscale 2013, 5 (9), 3601–3614. 10.1039/c3nr00476g. [PubMed: 23532413]

(56). Thomas AG; Syres KL Adsorption of Organic Molecules on Rutile TiO 2 and Anatase TiO 2 Single Crystal Surfaces. Chem. Soc. Rev 2012, 41 (11), 4207–4217. 10.1039/c2cs35057b. [PubMed: 22517475]

(57). Qi G; Liu X; Li C; Wang C; Yuan Z The Origin of Superhydrophobicity for Intrinsically Hydrophilic Metal Oxides: A Preferential O2 Adsorption Dominated by Oxygen Vacancies. Angew. Chemie - Int. Ed 2019, 58 (48), 17406–17411. 10.1002/anie.201909121.

(58). Panagiotou GD; Petsi T; Bourikas K; Garoufalis CS; Tsevis A; Spanos N; Kordulis C; Lycourghiotis A Mapping the Surface (Hydr)Oxo-Groups of Titanium Oxide and Its Interface with an Aqueous Solution: The State of the Art and a New Approach. Adv. Colloid Interface Sci 2008, 142 (1–2), 20–42. 10.1016/j.cis.2008.04.003. [PubMed: 18511015]

(59). Yang Y; Xu L; Dekkers S; Zhang LG; Cassee FR; Zuo YY Aggregation State of Metal-Based Nanomaterials at the Pulmonary Surfactant Film Determines Biophysical Inhibition. Environ. Sci. Technol 2018, 52 (15), 8920–8929. 10.1021/acs.est.8b02976. [PubMed: 30011188]

(60). Odling G; Robertson N Why Is Anatase a Better Photocatalyst than Rutile? The Importance of Free Hydroxyl Radicals. ChemSusChem 2015, 8 (11), 1838–1840. 10.1002/cssc.201500298. [PubMed: 25998373]

(61). Kim W; Tachikawa T; Moon G; Majima T; Choi W Molecular-Level Understanding of the Photocatalytic Activity Difference between Anatase and Rutile Nanoparticles. Angew. Chemie 2014, 126 (51), 14260–14265. 10.1002/ange.201406625.

(62). Buchalska M; Kobielusz M; Matuszek A; Pacia M; Wojtyła S; Macyk W On Oxygen Activation at Rutile- and Anatase-TiO2. ACS Catal. 2015, 5 (12), 7424–7431. 10.1021/acscatal.5b01562.

(63). Nosaka Y; Nosaka AY Generation and Detection of Reactive Oxygen Species in Photocatalysis. Chem. Rev 2017, 117 (17), 11302–11336. 10.1021/acs.chemrev.7b00161. [PubMed: 28777548]

(64). Sutton LE The Significance of the Differences between the Dipole Moments of Saturated and Unsaturated Substances. Proc. R. Soc. London. Ser. A, Contain. Pap. a Math. Phys. Character 1931, 133 (822), 668–695. 10.1098/rspa.1931.0174.

(65). Ighodaro OM; Akinloye OA First Line Defence Antioxidants-Superoxide Dismutase (SOD), Catalase (CAT) and Glutathione Peroxidase (GPX): Their Fundamental Role in the Entire Antioxidant Defence Grid. Alexandria J. Med 2018, 54, 287–293. 10.1016/j.ajme.2017.09.001.

(66). Ursini F; Maiorino M; Valente M; Ferri L; Gregolin C Purification from Pig Liver of a Protein Which Protects Liposomes and Biomembranes from Peroxidative Degradation and Exhibits Glutathione Peroxidase Activity on Phosphatidylcholine Hydroperoxides. Biochim. Biophys. Acta (BBA)/Lipids Lipid Metab 1982, 710 (2), 197–211. 10.1016/0005-2760(82)90150-3.

(67). Kedishvili NY; Goodwin GW; Popov KM; Harris RA Mammalian Methylmalonate-Semialdehyde Dehydrogenase. Methods Enzymol. 2000, 324 (1992), 207–218. 10.1016/s0076-6879(00)24233-x. [PubMed: 10989432]

(68). Liu S; Meng XY; Perez-Aguilar JM; Zhou R An in Silico Study of TiO2 Nanoparticles Interaction with Twenty Standard Amino Acids in Aqueous Solution. Sci. Rep 2016, 6 (August), 1–10. 10.1038/srep37761. [PubMed: 28442746]
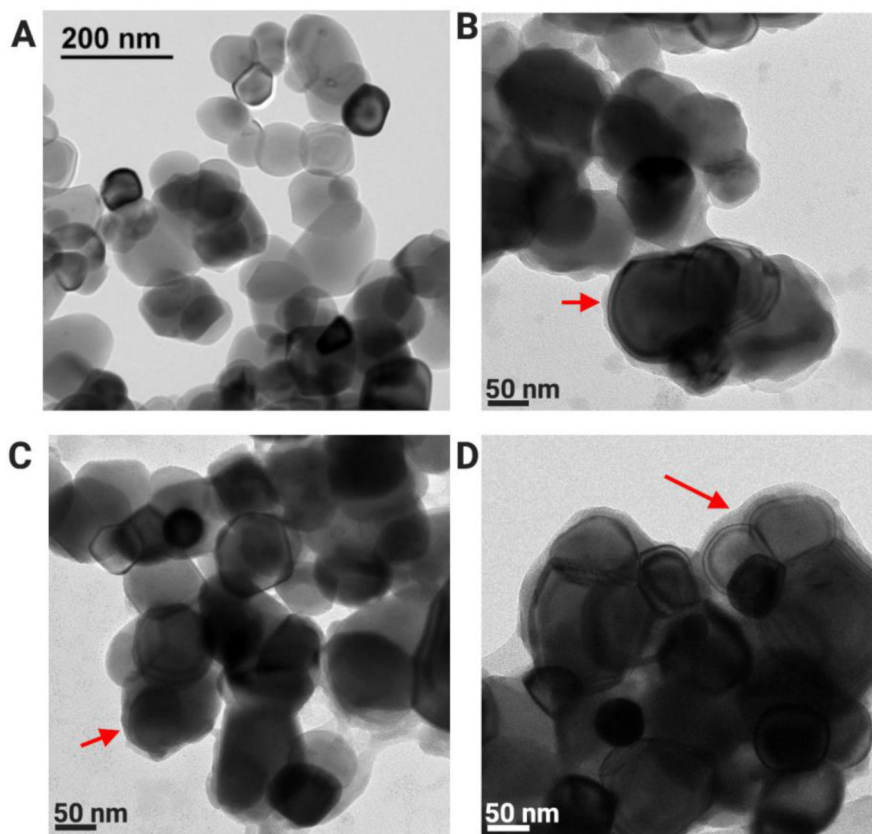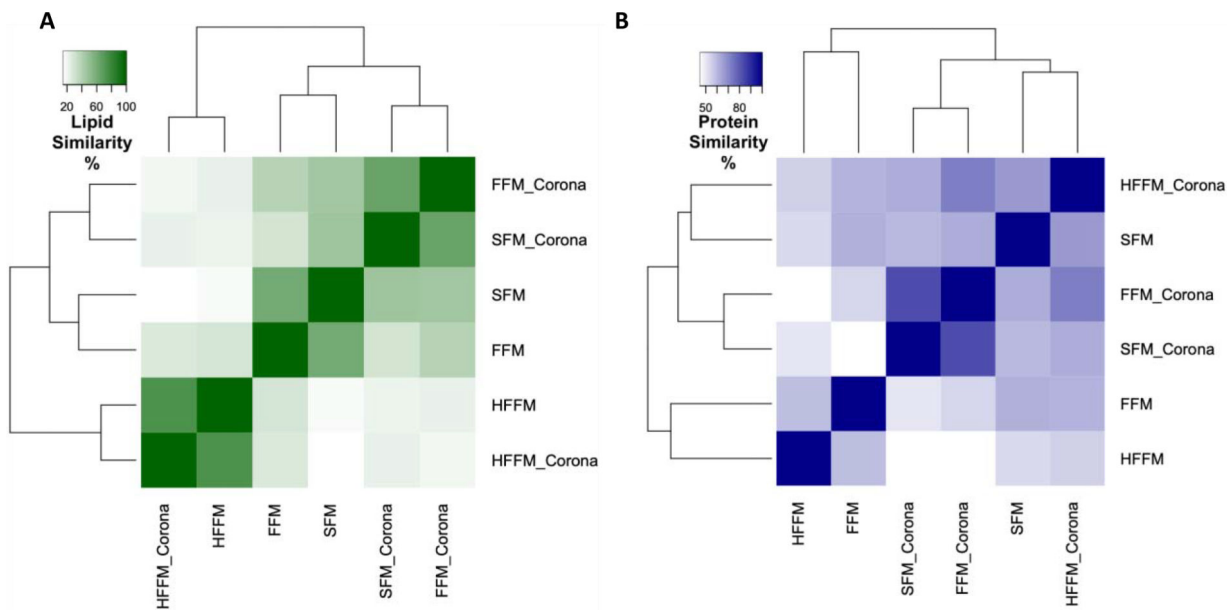
Figure 1.
TEM images of A) pristine E171 and digested E171 prepared with B) FFM, C) SFM, and D) HFFM. Red arrows denote the biocorona on the E171 surfaces. The image of A) pristine E171 was adapted from our previous work.
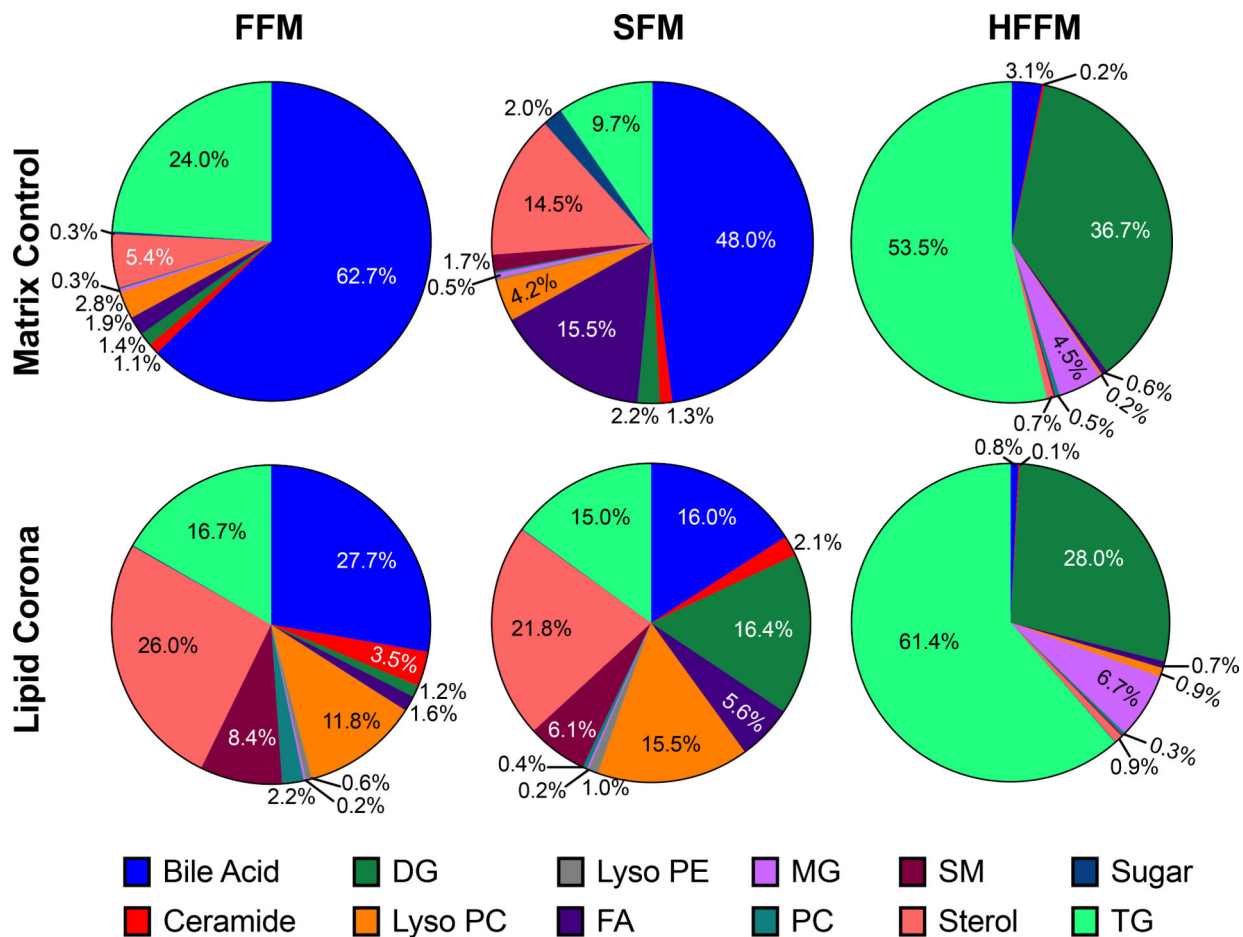
Figure 2.
Relative abundances of lipid classes identified in the three food model controls and the corresponding corona samples.
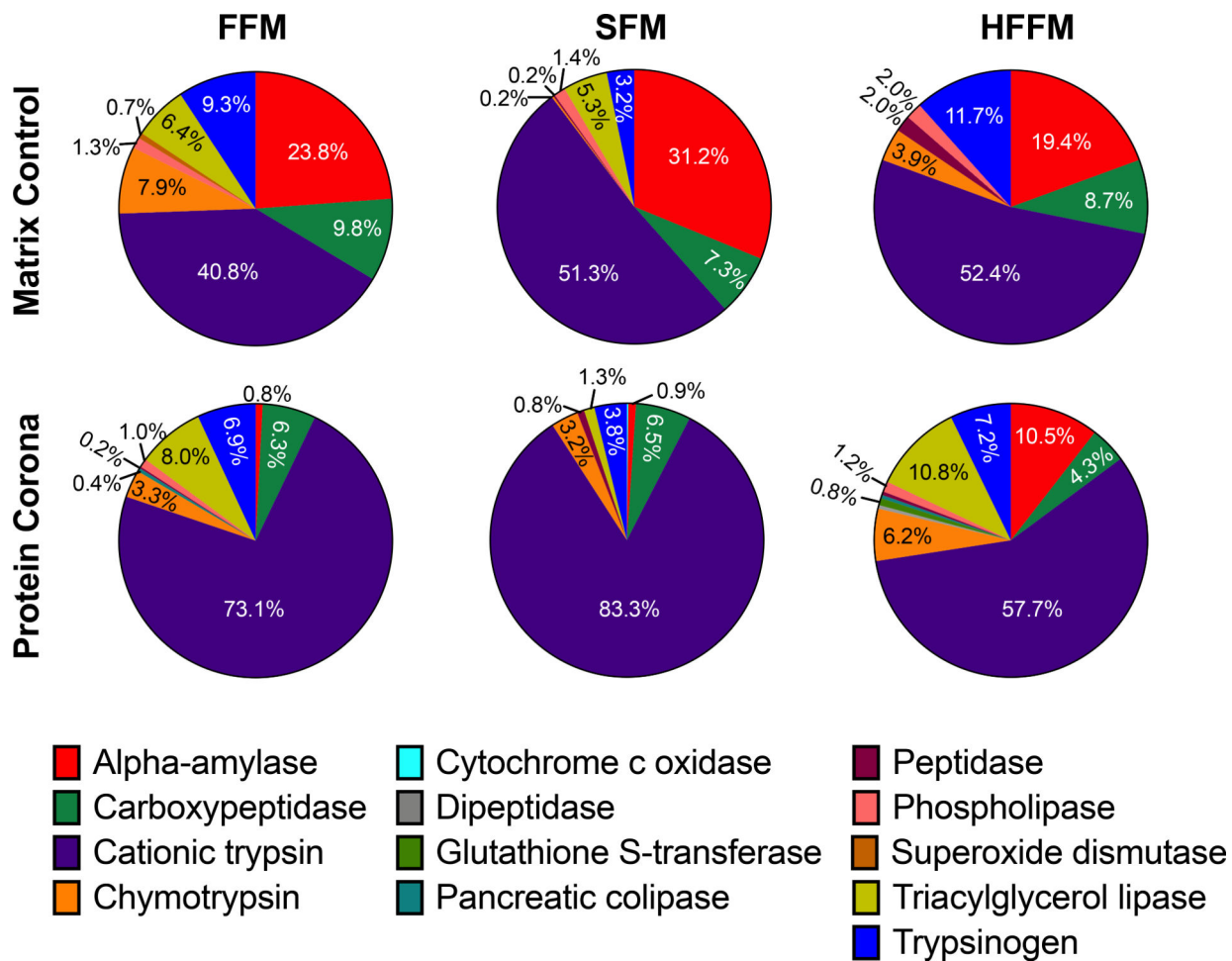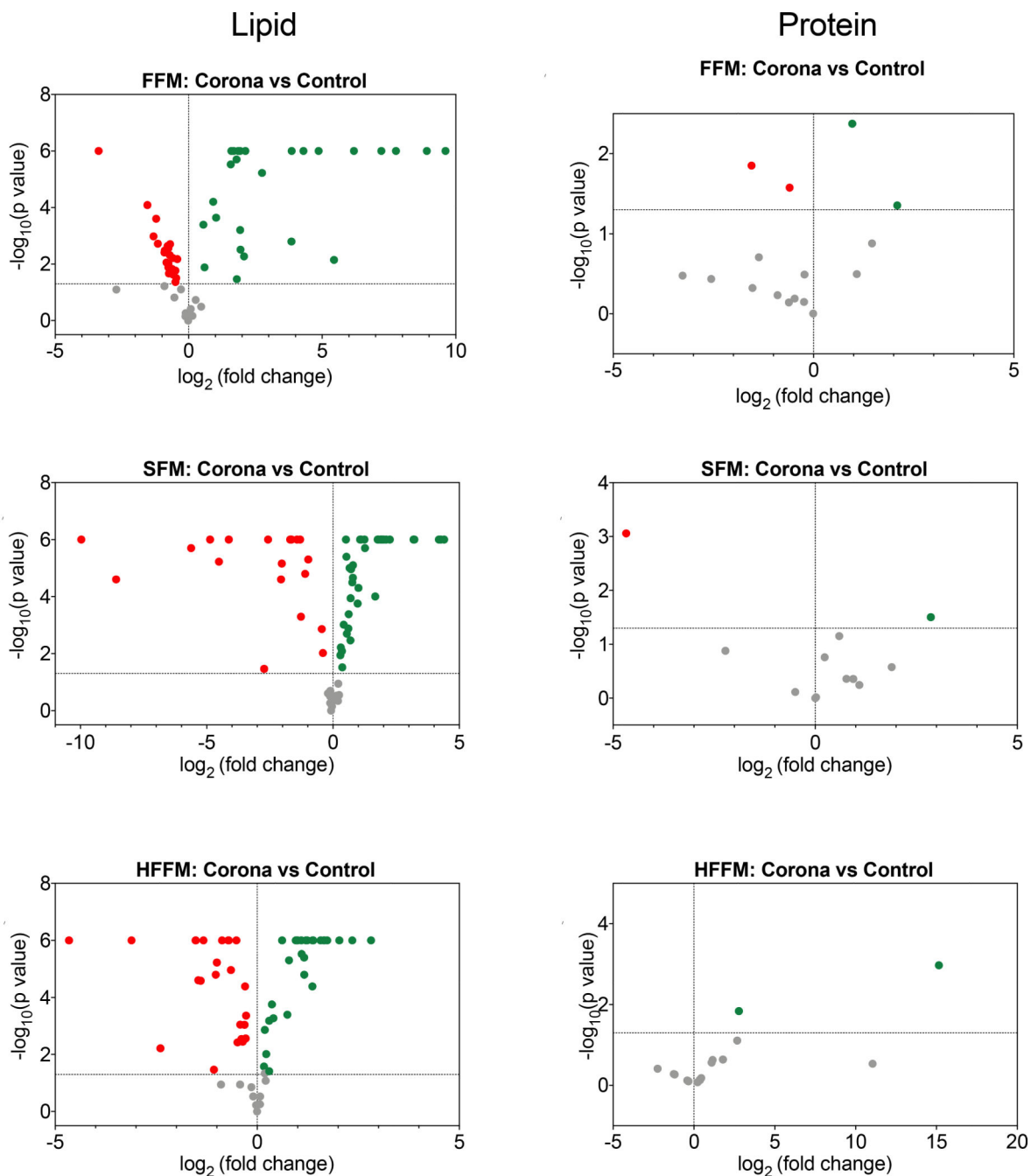
Figure 3.
Relative abundances of enzymatic proteins identified in the three food model controls and the corresponding corona samples. Six enzymes (17-beta-hydroxysteroid dehydrogenase, chymotrypsinogen, petidylpropyl isomerase, peroxiredoxin, protein kinase, and pancreatic ribonuclease) were not included in this figure as their relative abundances were low and considered negligible.

Figure 4.
Hierarchical cluster analysis of the similarities of A) lipid and B) protein compositions between food model controls and corresponding coronas. The unsupervised clustering confirms that there are more similar lipid and protein species between the FFM and the SFM digested samples (although values show less than 70% similarity), compared to the HFFM digestas (with values below 30% for lipids and 60% for proteins when compared to FFM and SFM).The similarity values were calculated from the average relative abundances between triplicate samples analyzed twice (n=6), while those for proteins were calculated from RA values from duplicate samples analyzed once (n=2). Dark green boxes indicate huge similarities between samples while white boxes signify trivial similarities.

Lipid

Protein

Figure 5.
The volcano plots compare the significantly enriched (green dots) or depleted (red dots) lipids and proteins in each food model. In these plots, the x-axis represents the fold change in lipid abundances in log_2 scale while the y-axis denotes the level of statistical significance between relative abundances (as −log (p value)). The dotted horizontal line at y = 1.3 designates the cutoff for significance. Dots above this line represent biomolecules with statistically significant abundances. The vertical line at x = 0 separates species that are enriched on the corona; dots to the right of this line represent enriched species and those that are to the left of the line are considered low affinity proteins. The low affinity proteins are
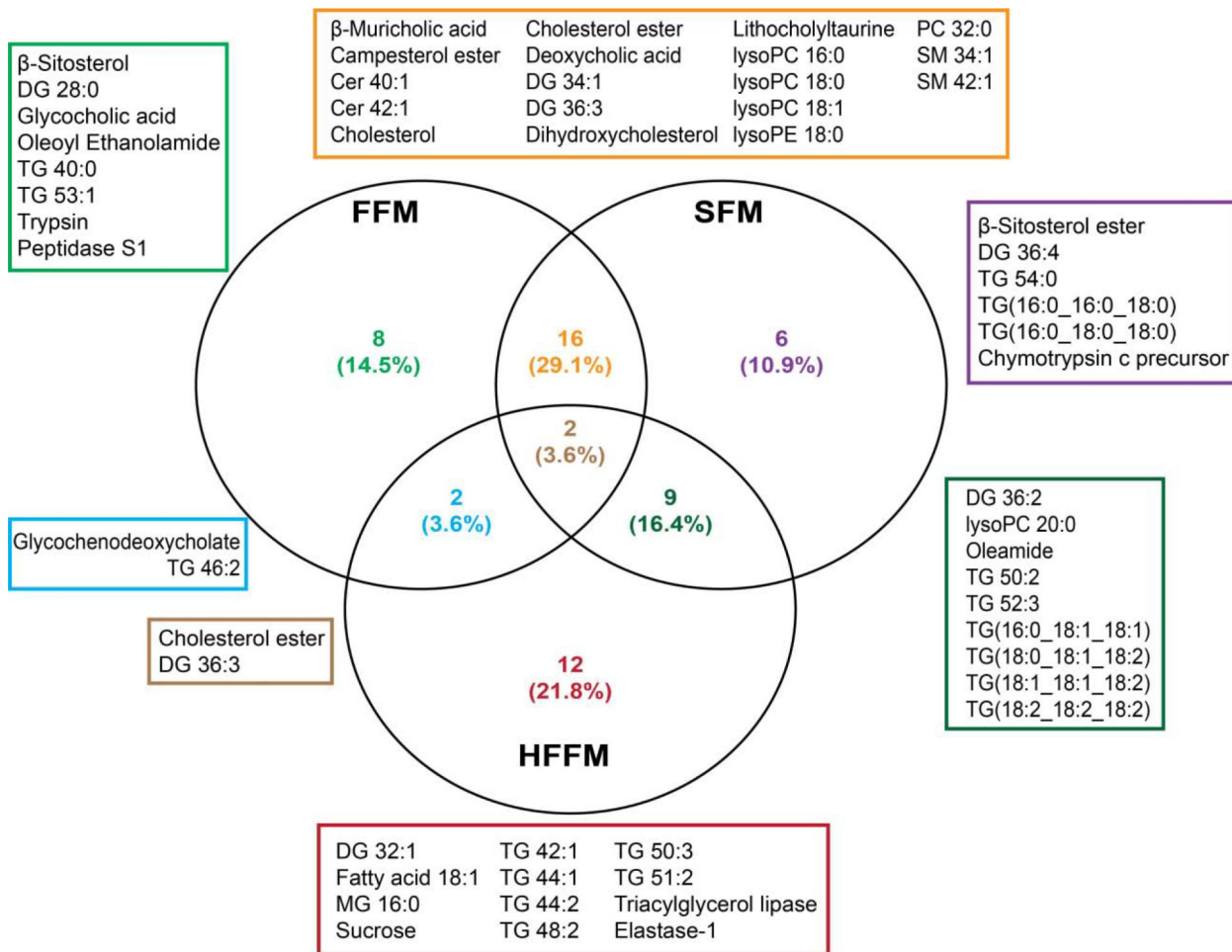
found in large abundances in the food model matrices. Therefore, the grey dots represent non-significant biomolecules.

Figure 6.
Quantitative Venn diagram showing the number of significantly enriched lipids in the TiO_2 corona for each food model. There were a total of 26, 32, and 23 enriched lipids for the FFM, SFM, and HFFM; 23, 16 and 43% of these lipids were distinctly adsorbed on the surfaces of TiO_2 after digestion with the respective food models. Two (cationic trypsin & peptidase S1 domain-containing protein), 1 (chymotrypsin c precursor), and 2 proteins (chymotrypsin-like elastase family member 1 (also known as elastase-1) & triacylglycerol lipase) were significantly enriched on the corona of the FFM, SFM, and HFFM, accordingly. There was no overlap of these proteins between the different food models.